Journal of Catalysis **190,** 92–103 (2000)
doi:10.1006/jcat.1999.2741, available online at http://www.idealibrary.com on IDEAL®

Microstructure and Characterization of a Highly Selective Catalyst for the Isomerization of Alkanes: A Molybdenum Oxycarbide

Christophe Bouchy, Cuong Pham-Huu, Baudouin Heinrich, Christian Chaumont, and Marc J. Ledoux[1]

Laboratoire de Chimie des Matériaux Catalytiques, GMI-IPCMS, ECPM/CNRS UMR 7504, Université Louis Pasteur (ULP), 25 rue Becquerel, BP 08, 67087 Strasbourg Cedex 2, France

Received June 10, 1999; revised October 22, 1999; accepted October 22, 1999

A molybdenum oxycarbide catalyst that is very active and selective for the isomerization of *n*-alkanes has been characterized by means of diffraction techniques and simulations. The proposed structure is confirmed by transmission electron microscopy. An elemental analysis performed on the pure phase prepared from a bronze precursor provides the stoichiometry of this new catalyst. Quantitative temperature-programmed oxidation measurements confirm the elemental composition. The stoichiometry of this new phase, $MoO_{2.42}C_{0.23}H_{0.78}$, shows an excess of light elements O, C, and H only possible because of the presence of metal vacancies. A tentative explanation of its peculiar catalytic properties is deduced from these structural and chemical features.

Key Words: **molybdenum oxycarbide; structure; alkanes isomerization; catalyst.**

INTRODUCTION

Analogies have been found between transition metal carbides (Mo_2C, WC, and/or W_2C) and metals of the platinum family (Pt, Rh, Ru). Their respective electronic structures and catalytic properties have induced much research both from a synthetic point of view and for potential catalytic applications (1–10). Among these, the selective isomerization of *n*-alkanes into branched isomers without aromatization or cracking is one of the most studied systems (6, 11, 12). Different authors have reported that, in general, transition metal carbides catalyze hydrogenolysis or cracking reactions better than selective isomerization (13–16). Iglesia *et al.* (6, 12, 17) have improved isomerization selectivity on tungsten carbides by inducing a slight oxidation of the surface by O_2 or air treatment. They suggested that the surface has a bifunctional aspect, with patches of carbide responsible for the dehydrogenation–hydrogenation of the alkane, and patches of acidic oxide responsible for the protonation and isomerization (bond shift), similar to what is observed on a conventional bifunctional catalyst such as Pt/acidic zeolite. At the same time, Ledoux *et al.* (18, 19) have suggested that the large improvement in isomerization selectivity observed when oxidizing the surface of Mo_2C was due to the formation of a new phase containing Mo, C, and O (and possibly H) atoms, and obtained by the reaction of the feed gas, a mixture of H_2 and hydrocarbon, partly re-carburizing the MoO_3 layer covering the top of the carbide's surface. The presence of Mo_2C in the bulk as support of this selective phase was probably not necessary. Indeed, starting from bulk MoO_3, it has been possible to prepare the same phase by reacting a flow of H_2/hydrocarbon directly with this bulk MoO_3 (20, 21).

This oxide, crystallizing in an orthorhombic system, exhibits a strong anisotropy (22) due to its lamelar structure made of bilayers of MoO_6 octahedra, bonded by van der Waals forces. At 350°C, regardless of the total pressure (from 1 to 40 atm), in the presence of H_2/hydrocarbon (ratio from 2 to 150), this oxide is readily transformed into two phases, the sub-oxide MoO_2 and this new oxycarbide phase, MoO_xC_y. The catalytic selectivity of this solid mixture is identical to that observed on the partly oxidized carbide. This selectivity is unique because it is the only catalyst able to isomerize long-chain ($\geq C_7$) linear alkanes into highly branched isomers at a very high conversion without cracking (19, 23, 24). This was attributed to the intervention of a reaction mechanism involving a metallacyclobutane intermediate (25) without any formation of carbocations, which thermodynamically favor the cracking of branched alkanes. The existence and the catalytic activity of this new oxycarbide are contested by different authors either attributing the activity to MoO_2 (26), although it has been shown that this sub-oxide is not selective for the reaction (27), or not choosing between MoO_2 and the oxycarbide (28). The difficulty arises from three facts. First, in the conditions used for its preparation, this oxycarbide is poorly, or not at all, crystallized (8), contrary to the well-crystallized MoO_2, rendering conventional X-ray diffraction (XRD) ineffective. Second, the degree of oxidation of Mo, +IV for MoO_2, lies between +IV and +V for the oxycarbide (8), making ambiguous the X-ray photoelectron spectroscopy (XPS) analyses of the surface. Third, this oxycarbide is stable in a reducing atmosphere containing hydrogen and/or

[1] To whom correspondence should be addressed. Fax: 33-388136880. E-mail: ledoux@cournot.u-strasbg.fr.

0021-9517/00 $35.00

hydrocarbon, but incorporates more carbon when heated above 400°C in the presence of a carbon source, to be transformed into another oxycarbide, not selective for alkane isomerization, already described in the literature (29); in an oxidizing atmosphere it is pyrophoric. The preparation of a pure single crystal to obtain an unambiguous structure was thus not a trivial task.

The objective of this article is both to describe the crystalline structure of this new phase by using a combination of simulations of powder XRD and microdiffraction performed in a transmission electron microscope (TEM) chamber, and to provide the stoichiometric composition of this material, obtained by quantitative temperature-programmed oxidation (TPO) performed on the pure phase. A new synthetic route leading to this pure phase is disclosed for the first time. This article is based on the Ph.D. work of C. Bouchy (30).

EXPERIMENTAL

The catalytic active phase in bulk form was obtained either mixed with MoO_2 when starting from bulk MoO_3 (Strem Chemicals, >99.5%) (20) or pure when starting from a hydrogen bronze of molybdenum oxide. In both cases the activation procedures were identical; i.e., the precursor (MoO_3 or the bronze) was treated by a flow of H_2 and *n*-heptane (molar ratio = 26, flow = 200 cc/min) at 350°C and a total pressure of 7 atm for a period of 24 h. It was verified that both preparations produced catalysts with identical properties for the *n*-heptane isomerization reaction. This provided an unambigous proof of the neutral role of MoO_2 on this reaction, as there was no trace of this oxide in the preparation when starting from the bronze; this was checked by HRTEM and XRD.

The bronze was prepared according to the method described by Glemser and Lutz (31). Five grams of MoO_3 powder (0.62 m^2/g) was introduced into an aqueous solution of HCl containing chips of Zn in slight excess, generating "native" hydrogen at their surface; these hydrogen atoms diffused between the layers of MoO_3 to form, depending on the concentration of HCl, either pure $H_{0.34}MoO_3$ with 3.5 cc of HCl (4 N), or mainly $H_{0.93}MoO_3$ with 8.7 cc of HCl (4 N). The slurry was washed many times in pure water in order to eliminate $ZnCl_2$ and unreacted HCl; Zn excess was manually separated. The final product was dried at 110°C and stored under nitrogen. Both materials were fully characterized by XRD, elemental analysis (no detectable Cl and 150 ppm of Zn), and BET specific surface area measurements (2.3 m^2/g for the two samples). Other routes (32) of anhydrous synthesis were also tested but did not show significant differences in the final result. In this article, only the experiments starting from pure $H_{0.34}MoO_3$ will be used.

Powder X-ray diffraction (XRD) was carried out on a Siemens model D-5000 diffractometer with Cu K_{a1} radiation ($\lambda = 0.15406$ nm). Before analysis, any air-sensitive materials were passivated by a mixture O_2/He 0.5%. Each material was finely ground in order to avoid preferential diffraction directions which could result from the formation of anisotropic microcrystals. This grinding was essential if one wanted to use the diffraction diagrams for comparison with simulations. It was checked that the "grinding" was effective, i.e., transformed an anisotropic system characterized by the high intensity of selected directions into an isotropic system where each line appeared with the expected intensity (p 64, Ref. 30).

Surface area and porosity measurements were carried out on a Coulter SA-3100 sorptometer with N_2 as adsorbent at liquid nitrogen temperature using the BET method. Before each measurement the sample was outgassed at 200°C for 1 h in order to desorb impurities on its surface.

Transmission electron microscopy (TEM) was carried out on a Topcon model E002B UHR operating at 200 kV equipped with a beryllium window, with a point-to-point resolution of 0.17 nm. To prevent artifacts due to contamination, no solvents were used at any stage and samples were prepared by grinding the material between glass plates and bringing the powder into contact with a holey carbon-coated grid. Selected area electron diffraction (SAED) was also used to assess the symmetry of the observed domains.

The simulation of the XRD diagrams and the SAED patterns were made with Ca.R.Ine Cristallographie 3.0 (Boudias & Monceau) software. It was possible to obtain theoretical diagrams and patterns from a crystallographic system and different parameters such as degree of substitution, number of vacancies, interstitial atoms, etc. The relative intensities of the different diffraction peaks could then be simulated.

Temperature-programmed oxidation (TPO) was performed *in situ* by a flow of O_2/He 10%, and the nature and the quantity of emerging products (H_2O, CO, CO_2) or the consumption of O_2 was followed by mass spectrometry (Varian Saturn III ionic trap mass spectrometer). The quantitative results were obtained by using standard references of products containing known amounts of C, O, and H, the surface area of a peak being proportional to the amount of the corresponding product.

RESULTS

XRD and HRTEM of the Mixture MoO_xC_y/MoO_2

The XRD diagram of the mixture is presented in Fig. 1. Narrow peaks corresponding to well-crystallized MoO_2 were identified by comparison with the JCPDS 32-0671 reference. Seven broader peaks were observed between $10° < 2\Theta < 100°$ which were attributed to MoO_xC_y. In addition, the strong noise observed as background could be the signal of a large proportion of an amorphous or poorly crystallized phase.

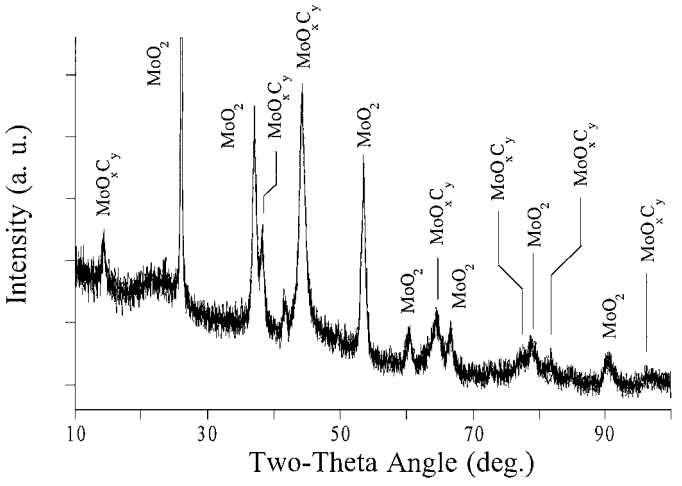

FIG. 1. X-ray diffraction diagram of activated MoO_3.

In Fig. 2a one can observe the presence of a well-crystallized phase, MoO_2, clearly identified both by direct measurements and by SAED (not reported), and of a second phase made of small aggregates, poorly crystallized. The SAED (top left corner) made on this phase corresponded to a cubic system (regardless of the sample and the orientation, only square patterns were ever observed) with relatively large spots, in agreement with a poor level of crystallinity. By increasing the resolution (Fig. 2b) it was, however, possible to exhibit a preferential orientation in the aggregates with an interplanar distance of 0.205 nm.

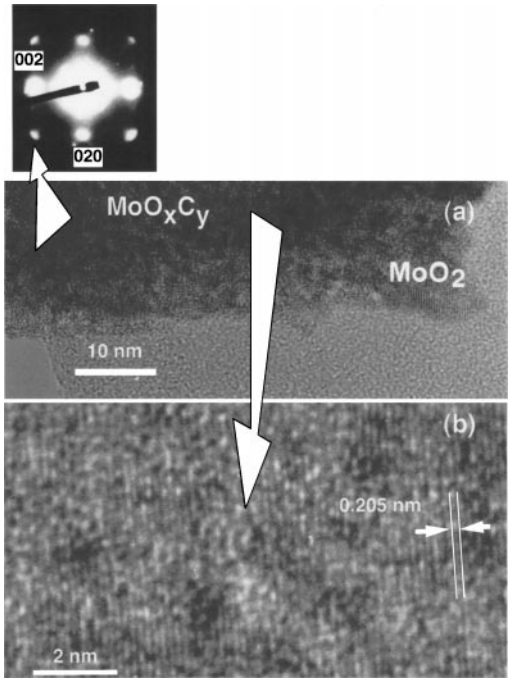

FIG. 2. Transmission electron microscopy (a, b) and selected area electron diffraction of MoO_xC_y.

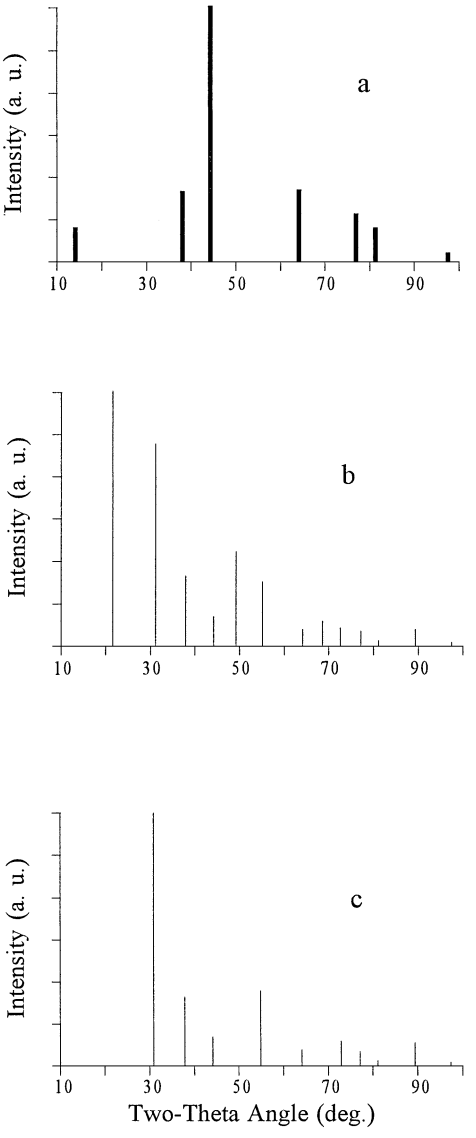

FIG. 3. X-ray diffraction, (a) measured and (b) simulated (for simple cubic and bcc systems).

Simulation of the XRD and SAED

The three cubic systems, i.e., simple, body-centered, and face-centered, were successively simulated in order to reproduce the XRD diagram corresponding to the experimental peaks attributed to the oxycarbide in Figs. 3a and 4a. A cubic unit cell parameter of 0.410 nm was selected from preceding TEM studies (8). For the simple cubic (Fig. 3b) and the body-centered cubic (Fig. 3c) systems the number of peaks was too high and could not be modified by varying the relative stoichiometry of the different elements, nor by introducing vacancies in the crystal networks. This was an indication that the crystallographic system probably had a higher symmetry.

The face-centered system was first simulated (Fig. 4b) for a stoichiometry Mo_2X, with X = C or O, isotypic of the

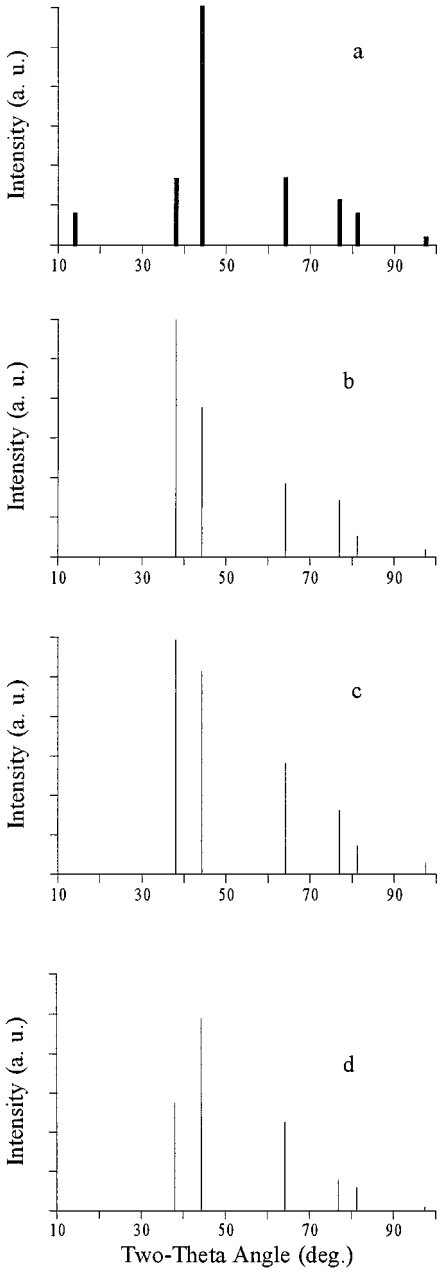

FIG. 4. X-ray diffraction, (a) measured and (b) simulated (for fcc system with different stoichiometries).

molybdenum nitride (γ-Mo_2N), with each metallic site at the nodes of the crystallographic network and the light elements (O and C) filling the octahedral voids with an occupancy probability of 0.5. The cell parameter of the nitride is slightly longer: 0.416 nm instead of 0.410 nm. It immediately appeared that the right number of experimental peaks (Fig. 4a) could be reproduced with the exception of the peak at very low angle (14.3°) (see Discussion). However, the relative intensities of the two main peaks did not fit and were, in fact, in a reverse ratio. Gouin *et al.* (33, 34) have shown for molybdenum nitrides that even if the contribution of the heavy atoms (Mo) is dominant in the intensity of the diffraction peaks, a change in the stoichiometry of the light atoms (N) can strongly affect the relative ratio of these intensities. This idea was applied to the MoO_xC_y material and different stoichiometries were consequently simulated.

Figure 4c simulates an XRD diagram where Mo atoms occupy all the nodes of the network and the light elements (O or C) fill all the octahedral voids (probability = 1), stoichiometry MoX, with the cell parameter still fixed at 0.410 nm. The intensities of the two main peaks were still not in the right ratio.

In a Hägg (35) compound the light elements C, O, and N can be found only in the octahedral vacancies or voids of the metal crystal network. Consequently, the stoichiometry MoX_2 can be obtained only if all the octahedral voids are filled with the light elements and if the nodes of the network are occupied by the heavy metal with a probability of 0.5 without predetermined organization of the vacancies. Introducing this atomic spatial distribution and with a cell parameter of 0.410 nm, it was then possible to obtain an excellent fit between the measured and simulated XRD diagrams (Fig. 4d). A predetermined organization of the occupied nodes or of the metal vacancies, which is the same thing, should increase the number of reflections in the diagram. These results and the indices of each peak are summarized in Table 1. Two points should be underlined: the peak observed at 0.619 nm was not obtained by any simulation, and the introduction of hydrogen atoms in the structure did not modify the intensity of the diffraction peaks.

It was then possible to interpret the SAED which is presented in Fig. 2a (top left corner). The square symmetry of the spots indicated that the microcrystals were mainly

TABLE 1

Comparison between the Experimental and Simulated XRD Patterns of the Molybdenum in the Face-Centered Cubic System with Different Metal-to-Light Elements Ratios MoX : Mo_2X and $a = 0.410$ nm

Experimental (Fig. 4a) d, nm/I/I_0	MoX_2 (Fig. 4d) d, nm/I/I_0/(hkl)	MoX (Fig. 4c) d, nm/I/I_0/(hkl)	Mo_2X (Fig. 4b) d, nm/I/I_0/(hkl)
0.6188/12			
0.2366/27	0.2367/56/(111)	0.2367/100/(111)	0.2367/100/(111)
0.2047/100	0.2050/100/(200)	0.2050/88/(200)	0.2050/63/(200)
0.1449/27	0.1450/46/(220)	0.1450/42/(220)	0.1450/31/(220)
0.1236/17	0.1236/16/(311)	0.1236/25/(311)	0.1236/24/(311)
0.1184/12	0.1184/12/(222)	0.1184/11/(222)	0.1184/8/(222)
0.1025/—[a]	0.1025/5/(400)	0.1025/5/(400)	0.1025/4/(400)
0.0941/—[a]	0.0941/7/(331)	0.0941/10/(331)	0.0941/9/(331)
0.0917/21	0.0917/15/(420)	0.0917/15/(420)	0.0917/15/(420)

[a] Too small intensity to be detected; however, some very weak signals can be observed at these angles on Fig. 1.

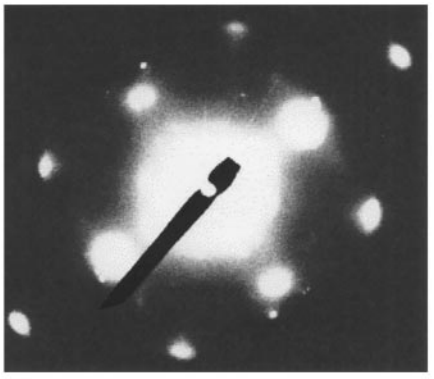

Experimental Selected Area Electron Diffraction (SAED)

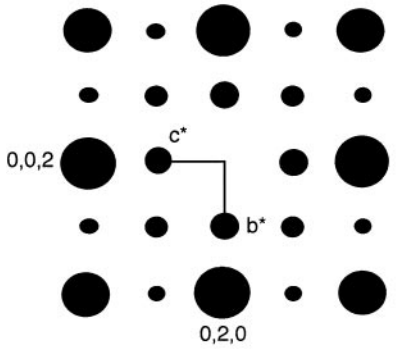

1st simulation
fcc, zone axis [100]
(d.o. = degree of occupancy) :

Mo (0 / 0 / 0) and equivalent:
d.o. = 100%
Mo (0,5 / 0,5 / 0) and equivalent:
d.o. varied from 0 to 100%

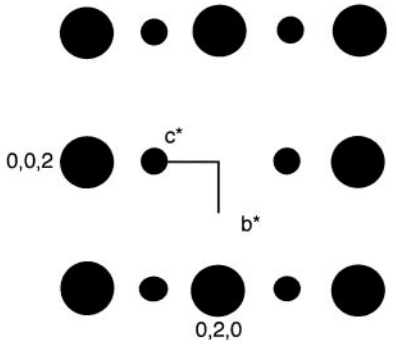

2nd simulation
fcc, zone axis [100]
(d.o. = degree of occupancy) :

Mo (0 / 0 / 0) and eq.: d.o. = 100%
Mo (0 / 0,5 / 0,5): d.o. = 100%
Mo (1 / 0,5 / 0,5): d.o. = 100%
Mo (0 / 0,5 / 0,5): d.o. = 0%
Mo (0,5 / 0 / 0,5): d.o. = 0%
Mo (0,5 / 0,5 / 1): d.o. = 0%
Mo (0,5 / 1 / 0,5): d.o. = 0%

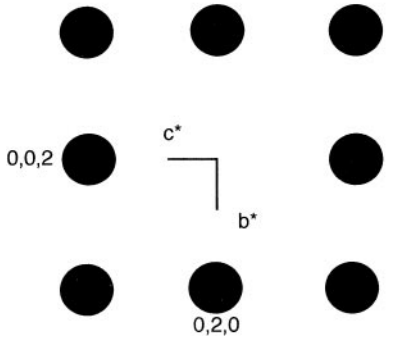

3rd simulation
fcc, zone axis [100]
(d.o. = degree of occupancy) :
For all sites : d.o. = 50%

FIG. 5. Selected area electron diffraction, measured and simulated (with different stoichiometries).

oriented along the [001] zone axis, the measured interreticular distances corresponding to the [200] (0.205 nm) and [220] (0.145 nm) reflections. The results of the SAED simulation for different degrees of occupancy of the metal sites are shown in Fig. 5. It was clear that the correct fit was obtained when the vacancies were not organized (third simulation with a probabilistic distribution of the metal atoms of 0.5 per site). A consequence of this probable distribution was the nonequivalence in terms of metal environment of each metal site. But in this case the reflections of uneven orders [100], [101], . . . should be observed with a fcc structure, which was not obvious at first sight. However, a careful examination of the central spot of the photograph showed a star shape, suggesting that very probably the [100] and/or [101] diffused reflections were making the branches of this star.

Direct HRTEM of a Well-Crystallized Microcrystal of the Molybdenum Oxycarbide MoO_xC_y

In order to confirm the results of the different simulations it was necessary to have a direct view of the well-crystallized material. The preparation of MoO_xC_y supported on SiC for an industrial application (36, 37) gave the opportunity to obtain well-crystallized microcrystals. MoO_3 supported on SiC was flash-heated in a few seconds from room temperature to 550°C in a flow of H_2/butane (molar ratio 9/1) and then cooled to room temperature. The result was the formation of MoO_2 and well-crystallized needles of MoO_xC_y. Figure 6 shows a HRTEM picture of one of these needles. Luckily this particle presented an easily recognizable macle in the middle of the photograph, between two parts of a microcrystal of different orientations, one with a pseudohexagonal symmetry and the other with a square symmetry. Both had the characteristic angles and distances of a fcc system, with a unit cell parameter equal to 0.410 nm.

So, from the pseudohexagonal symmetry it was possible to measure an interplanar distance of 0.23 ± 0.01 nm for two families of planes making an angle of $70 \pm 1°$. From the square symmetry it was possible to find interplanar distances of 0.21 ± 0.01 or 0.43 ± 0.01 nm making an angle of 90°. These parameters correspond to the distances and angles of the (111), 0.237 nm, (200), 0.205 nm, and (100), 0.410 nm planes of a fcc crystal with $a = 0.410$ nm. The pseudohexagonal grain was oriented along the [110] zone axis, while for the square grain it was the [100] zone axis along which it was observed. A careful examination of this last grain showed in certain places columns of atoms materializing the fcc symmetry of the system.

XRD and TPO of the Pure MoO_xC_y Phase

As explained above, it was possible to prepare the MoO_xC_y phase without the presence of MoO_2 by treating $H_{0.34}MoO_3$ with a flow of H_2/hydrocarbon. The XRD diagram of the oxycarbide obtained with a mixture of

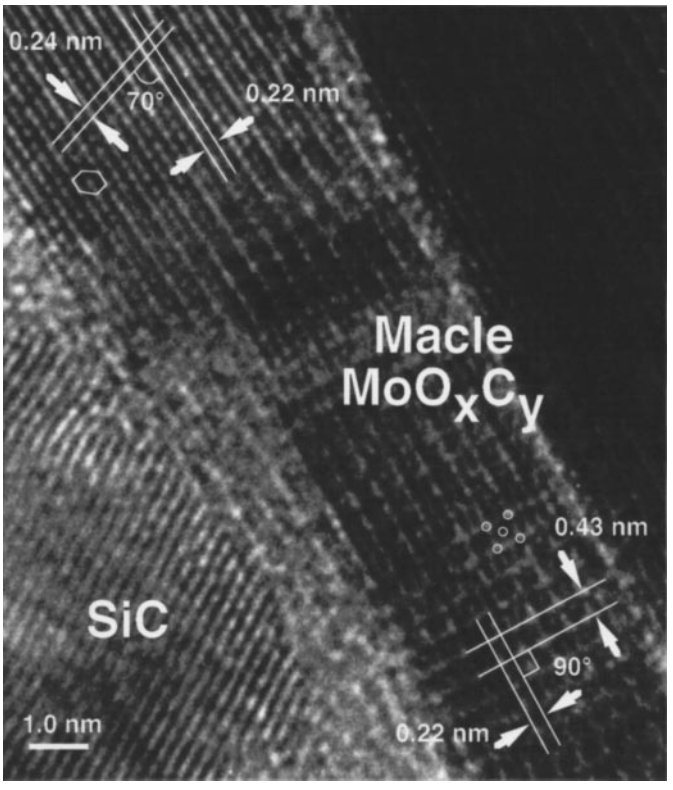

FIG. 6. High-resolution transmission electron microscopy of a MoO_xC_y microcrystal.

H_2/butane at 1 atm is reported in Fig. 7. Only the broad (200), (110), and (220) diffraction peaks were visible. The very high level of background noise witnessed the poor crystallinity of the material. The very intense peak of MoO_2 at $2\Theta = 26°$ was not observable. The unknown peak at $d = 0.618$ nm ($2\Theta = 14°$) was the second highest in intensity.

In Fig. 8b the temperature-programmed oxidation (TPO) diagram of this material is reported. The oxidation was violent: a single narrow peak of emitted CO_2 coincided with the peak of oxygen consumption. A second very small, broad peak followed the first one and could correspond to trace

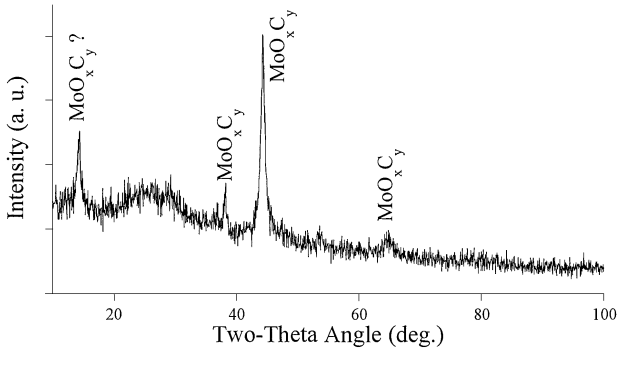

FIG. 7. X-ray diffraction diagram of pure MoO_xC_y obtained by activation of the bronze $H_{0.34}MoO_3$.

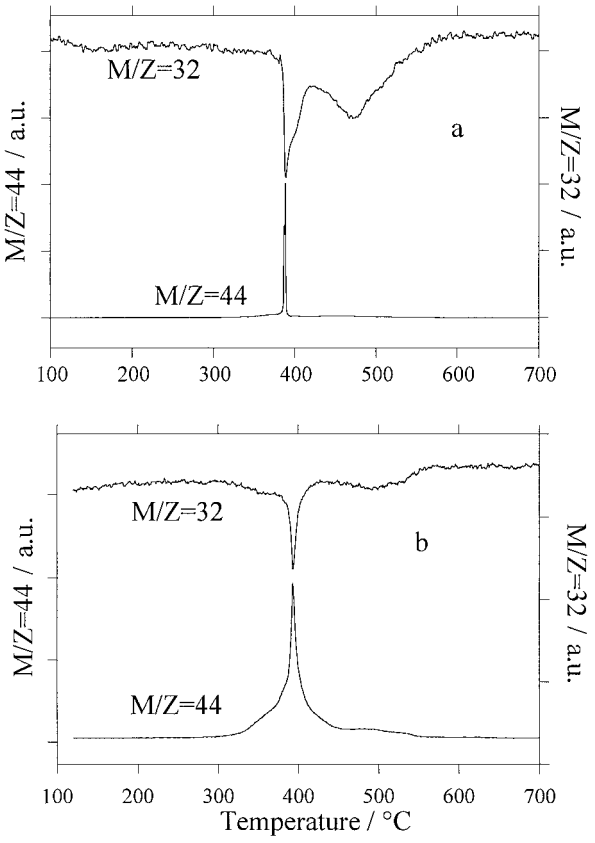

FIG. 8. Temperature-programmed oxidation of (a) the mixture $MoO_xC_y + MoO_2$ and (b) pure MoO_xC_y.

amounts of MoO_2 or adsorbed carbon coming from the activation operation. In comparison to the material obtained when bulk MoO_3 was used as starting product, the mixture of oxycarbide and MoO_2 was clearly identified (Fig. 8a). The diagram of oxygen consumption showed three parts: a sharp peak corresponding to the combustion of the oxycarbide into MoO_3 with the release of CO_2, a shoulder of this peak probably corresponding to the oxidation of Mo contained in the oxycarbide part of the mixture without CO_2 release (an XRD performed at this stage of oxidation showed that MoO_xC_y was totally transformed into MoO_3, leaving untouched MoO_2), and a broad peak corresponding to the oxidation of MoO_2 into MoO_3 without release of CO_2. The oxidation of Mo +IV and +V into Mo +VI is a slower reaction than the explosive oxidation of the oxycarbide and explains why the peaks corresponding to the metal oxidation were broader than the peak of carbon combustion.

The small shoulder observed before the peak corresponding to the pure oxycarbide in Fig. 8b was attributed to traces of adsorbed carbon or coke as identified from a material purposely covered by coke (not shown). By integrating the surface of the peaks corrected from the small amounts of MoO_2 and coke and using the calibration curve established under the same conditions with known amounts of carbon and oxygen, it was possible to calculate the stoichiometry of the sample: $MoO_{2.37}C_{0.32}$. The formation of H_2O during the TPO was diffuse and did not correspond to a well-characterized peak. Consequently, the only possibility to measure the H stoichiometry was elemental analysis, which gave $MoO_{2.42}C_{0.23}H_{0.78}$, in very close agreement with the TPO result. The absence of a clear peak of water desorption suggested that hydrogen was not forming a unique chemical bond with the substrate but more probably was occupying interstitial sites in the structure. The same quantitative measurement made on the material obtained from bulk MoO_3 produced a stoichiometry of $MoO_{2.34}C_{0.10}H_{1.38}$. Here, the peak corresponding to water emission was well resolved, allowing the evaluation of the H content.

DISCUSSION

The crystallographic symmetry adopted by the atoms in the oxycarbide prepared at 350°C was isostructural to nitrides, carbides, and other oxycarbides prepared at higher temperatures. However, the cell parameter was significantly shorter in the new compound, 0.410 nm instead of 0.416 to 0.424 nm (see Table 2 and references therein). It was shown (see Fig. 9) that the cell parameter increased with the degree of carburation and that an oxycarbide of Mo prepared at 550°C had a structure and a stoichiometry very close to those of a carbide, catalytic properties equivalent to the properties of Mo_2C, and a cell parameter equal to 0.418 nm. Lee *et al.* (39) had observed a similar evolution during the preparation of α-MoC_{1-x}, with x close to 0.5, $a = 0.424$ nm, while an intermediate product of synthesis, an oxycarbide of Mo, had a parameter equal to only 0.418 nm. The smaller value of the parameter for the oxycarbide phase when compared to those of conventional nitrides and carbides was the sign of a low content of carbon and was certainly due to the low temperature of synthesis.

Apart from this short parameter, the understoichiometry in metal was also remarkable. The usual syntheses of Mo carbides and nitrides are generally performed at high temperatures above 750°C, without intermediate stages at

TABLE 2

Cell Parameters of the Nitride, Carbide, and Oxycarbide of Molybdenum Crystallized in the Face-Centered Cubic Structure

Compound	Cell parameter, nm	Ref.
γ-Mo_2N	0.416–0.420	33
$MoO_{0.46}C_{0.28}$	0.417	38
$MoO_{0.31}C_{0.34}$	0.418	38
MoO_xC_y (250°C)[a] (made from Pt(0.25%)/MoO_3)	0.418	39
α-MoC_{1-x}	0.424	39
oxycarbide (350°C)	0.410	This work
oxycarbide (550°C)	0.418	40

[a] Calculated from diffraction angles given by the authors.

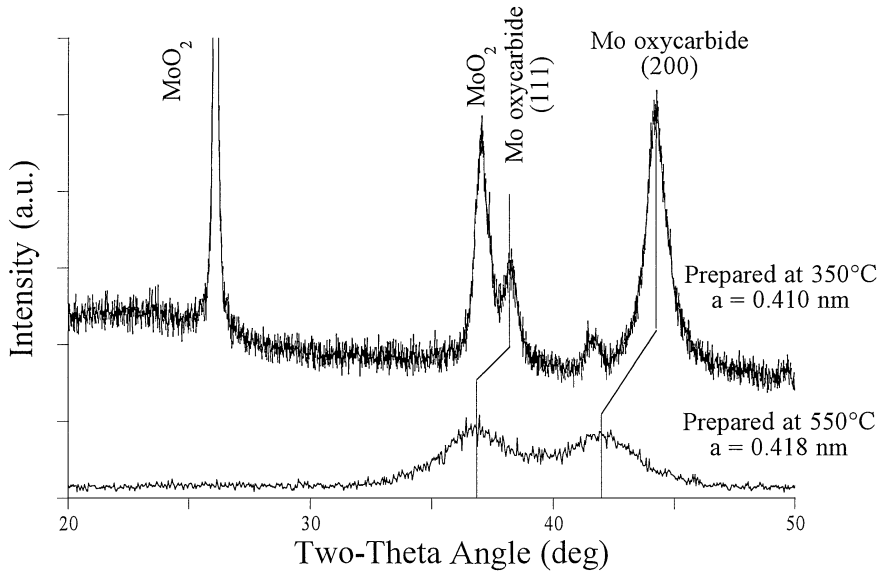

FIG. 9. Expansion of the cell parameter according to the degree of carburation observed by XRD.

constant lower temperatures; they all produce high-density materials with upper stoichiometries in metal such as Mo_2C, for instance. This is due to the high mobility of the metal atoms when temperature is increased; to obtain low-density material with a large amount of metal vacancies it was thus important to work at relatively low temperatures. The difference observed between 350 and 550°C in Fig. 9 was very demonstrative. The increase in density or in metal concentration not only shortened the cell parameter but also inverted the intensity ratio between the diffraction planes (111) and (200), which was well consistent with an increase of the metal density in the (111) planes. The understoichiometry in metal had already been observed by Yu and Oyama (41) during the synthesis of bimetallic oxynitrides of W and V, even if this synthesis was performed at high temperatures, up to 750°C. This was probably due to the lower mobility of W and V atoms when compared to that of Mo alone. The atomic ratio between the light elements (O and N) and the metals (V and W) was found to be as high as 2.16 compared to 1 in VN or WN. Remarkably, they also found a relatively short cell parameter for a fcc structure, $a = 0.413$–0.414 nm.

All the peaks observed in the XRD diagram of the oxycarbide could be indexed as peaks belonging to a fcc structure with the exception of the peak corresponding to an interplanar distance of 0.619 nm. It was noted that this peak was very intense at the beginning of the synthesis, the highest after 3 h, and decreased to almost disappear after 50 to 60 h. The corresponding plane, reminiscent of the initial layered anisotropic structure of MoO_3, could contain an organization of the metal vacancies every four planes of the (010), (100), or (001) families because $0.410 \times 1.5 = 0.615$ nm, close to the measured distance of 0.619 nm (see Fig. 10b) (42). The vacancies, which were probably well

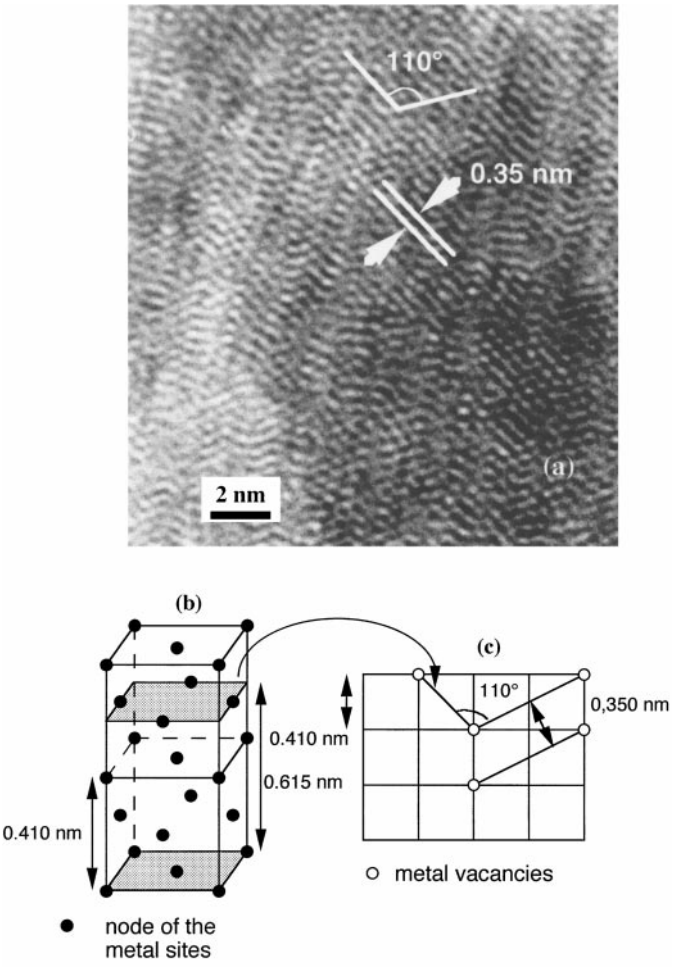

FIG. 10. Superstructure due to the pseudo-organization of the metal vacancies. (a) High-resolution transmission electron microscopy; (b) three-dimensional structure of the metal sites; and (c) projection on the plane (100).

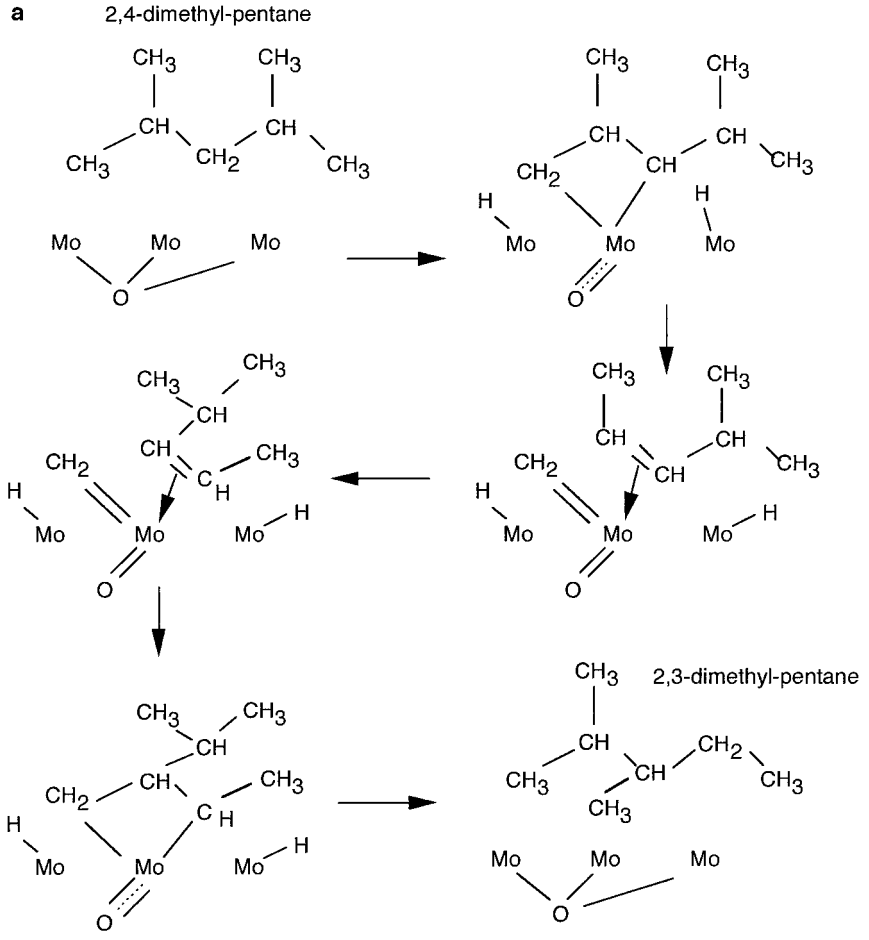

FIG. 11. Mechanisms of reaction: (a) metallacyclic intermediate and (b) conventional bifunctional.

organized for the sake of thermodynamic stability at the beginning of the MoO_3 reduction and because of the topotactic character of the transformation, could be progressively disorganized with a probable distribution when the time under reactive gas flow was increased. This could explain the peculiar structure in a "chevron"-type pattern observed by TEM during the formation of the oxycarbide (Fig. 10a). The measured distance, 0.350 nm, and the measured angle, 110° (Fig. 10c), clearly corresponded to a short distance order in the pre-fcc structure precursor of the final fcc with a probable distribution of the vacancies.

At the beginning of this article, the exclusive property of this material for the isomerization of *n*-alkanes was underlined. Is it possible to correlate this property with the new information collected on the structure of the active solid? On a conventional bifunctional catalyst the isomerization mechanism proceeds through five steps (Fig. 11b): the dehydrogenation on the metallic site, followed by the protonation and cyclization of the olefin on the acidic site, the bond shift by ring opening, the deprotonation to form a new olefin, and finally, the hydrogenation of this last olefin. This process can be repetitive but when the branching of the molecule is too high the ring opening step leads to the cracking of the molecule because the cracked fragments are thermodynamically more stable than the molecular carbocation (43). The mechanism, which involves a metallacyclobutane ring as intermediate (25, 44, 45), is not limited by the thermodynamic stability of cations because it does not involve in its process the intervention of any ionic species (Fig. 11a). Boudart and Ptak (44) have shown by checking most of the transition metals that neopentane was isomerized only on Pt, Ir, and Au catalysts, and consequently only these metals were able to form a metallacyclobutane intermediate, as it is the only route which allows the isomerization of this hydrocarbon in normal catalytic conditions of reaction. These three transition metals crystallize in the fcc symmetry, while earlier transition metals such as Mo, V, and W prefer the bcc symmetry. The theory of Engel and Brewer (46) suggests that the crystallographic system of a metal is correlated to its electronic structure. This electronic structure is one of the determining parameters of the catalytic properties of the metal. Consequently, one should not expect equivalent properties for Mo (bcc) and Pt (fcc). However, the adoption of the fcc

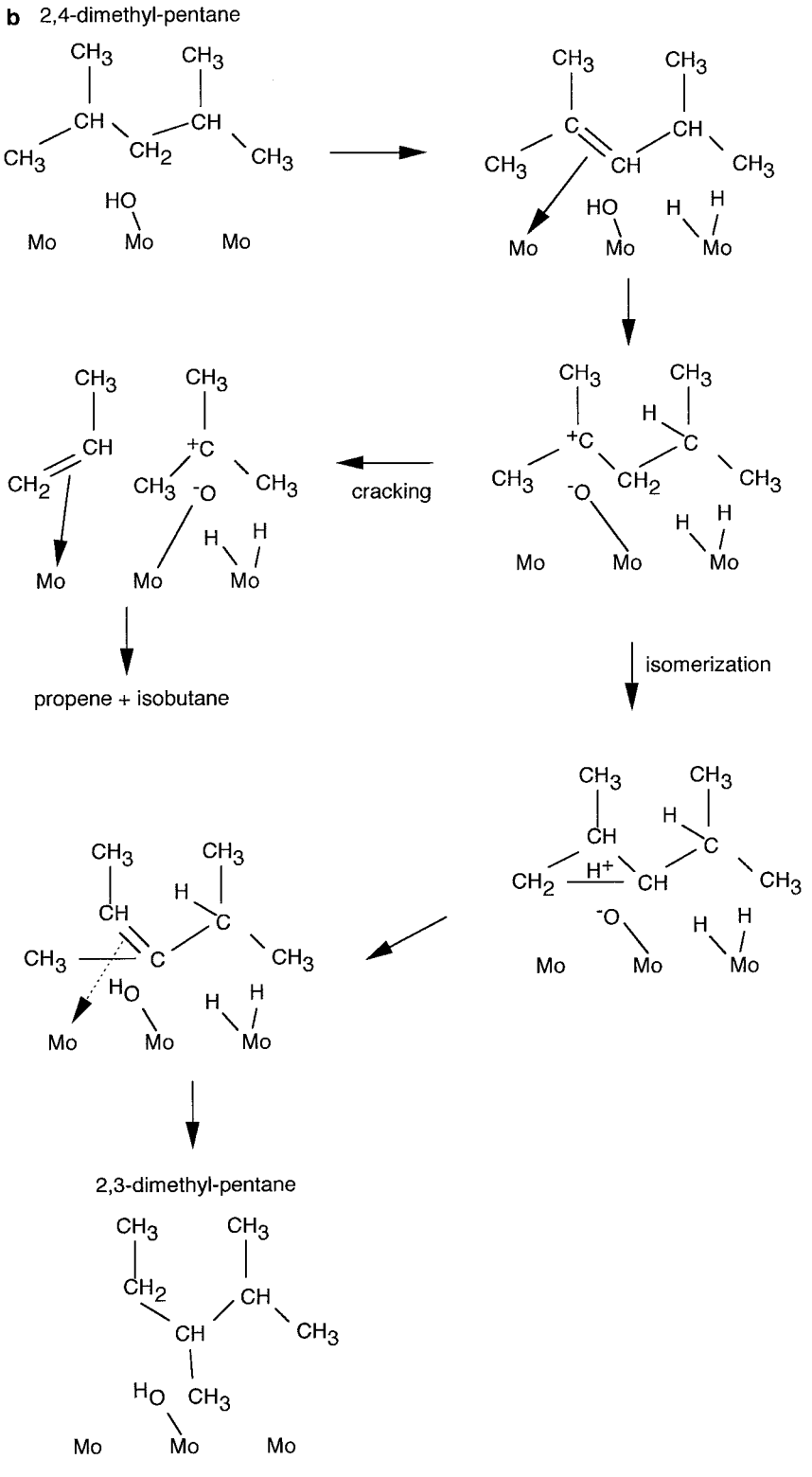

FIG. 11—*Continued*

symmetry by the Mo carbides and oxycarbides indicates that the electronic structure of Mo has been modified in the direction of the Pt (Ir, Au) structure and now one should expect a closing of the gap between the catalytic properties.

Many other parameters govern the catalytic behavior; among them the surface order is very important, especially for a structure-sensitive reaction such as the selective isomerization of alkanes. The new Mo oxycarbide contains large amounts of metal vacancies giving room and free access of the adsorbed reactants to the remaining metal atoms. In addition, the presence of high concentrations of oxygen atoms can favor the formation of the metallacycles by trapping the excess of free electrons of the Mo surface atoms in Mo_2C, too many electrons and vacancies favorizing too much the multiple adsorption of the hydrocarbon, the precursor of an extensive hydrocracking. Moreover, Rappé and Goddard (47) have clearly shown that in the olefin metathesis mechanism, equivalent to the metallacyclic mechanism proposed here, the oxygen ligand is intimately involved in the catalytic processes on high-valent Mo complexes. This is consistent with the role of oxygen observed in the heterogeneous system.

In summary, the catalyst is a sub-oxide of Mo containing many vacancies. The role of the carbon atoms should be to stabilize a metastable intermediate phase between MoO_3 and MoO_2 by blocking the shearing process where the organization of the vacancies formed by H_2 reduction of MoO_3 allows the collapse of the MoO_3 orthorhombic layered structure into the more dense monoclinic structure of MoO_2 (48). The process is comparable to that described by Spevack and McIntyre (49), who showed that during the transformation of MoO_3 into MoS_2 sulfur atoms followed the preferential pathways of the shear planes to penetrate the layered structure and form intermediate sulfoxides.

One point remains unclear. During the transformation of MoO_3 into MoO_xC_y, the surface area of the material increases from 4 to 140 m^2/g (80–90 m^2/g after passivation) and this porous system contains a relatively large amount of micropores (60% of the total pore volume). These micropores could introduce a shape selectivity similar to that observed on Pt/H–ZSM22 (50) for instance and be another explanation for the very high selectivity observed during the isomerization of long-chain *n*-alkanes. This geometric effect is currently being studied on model catalysts where micro- and nanopores are controlled.

CONCLUSION

A thermal and chemical treatment of MoO_3 could generate a very active and selective catalyst for the isomerization reaction of alkanes. The control of the temperature at a relatively low level, 350°C, and of the gas flow, a mixture of H_2 and an hydrocarbon, could provide a solid mixture containing inactive MoO_2 and a molybdenum oxycarbide, $MoO_{2.42}C_{0.23}H_{0.78}$. The structure and the stoichiometry of this new phase was confirmed by the use of different techniques: X-ray diffraction, simulation, electron microscopy and diffraction, elemental analysis, and quantitative temperature-programmed oxidation. This active catalyst could be prepared as a pure phase without the presence of parasitic MoO_2 by starting from a bronze of molybdenum, $H_{0.34}MoO_3$. The high selectivity obtained on the catalyst was attributed to the intervention of a mechanism involving a metallacyclic intermediate, avoiding the negative role of the carbocation intermediates which favor the cracking reaction of the highly branched alkanes on conventional bifunctional catalysts. The presence of metal vacancies and the high concentration of oxygen stabilized the metallacyclic adsorbed species, the role of the carbon being to stop the evolution or the collapse of the structure during the hydrogen reduction of MoO_3 into MoO_2.

REFERENCES

1. Muller, J. M., and Gault, F. G., *Bull. Soc. Chim. Fr.* **2**, 416 (1970).
2. Boudart, M., and Levy, R., *Science* **181**, 547 (1973).
3. Oyama, S. T., and Haller, G. L., "Surface and Defects Properties of Solids, Specialist Periodical Reports," Vol. 5, p. 333. The Chemical Society, London, 1982.
4. Leclercq, L., *in* "Surface Properties and Catalysis by Non-Metals" (J. P. Bonnelle, B. Delmon, and E. G. Derouane, Eds.) NATO ASI Series, p. 433. 1983.
5. Lee, J. S., Oyama, S. T., and Boudart, M., *J. Catal.* **106**, 125 (1987).
6. Ribeiro, F. H., Dalla Betta, R. A., Boudart, M., Baumgartner, J. E., and Iglesia, E., *J. Catal.* **130**, 86 (1991).
7. Ledoux, M. J., Pham-Huu, C., Guille, J., Dunlop, H., Hantzer, S., Marin, S., and Weibel, M., *Catal. Today* **15**, 263 (1992).
8. Delporte, P., Meunier, F., Pham-Huu, C., Vennégues, P., Ledoux, M. J., and Guille, J., *Catal. Today* **23**, 251 (1995).
9. Oyama, S. T., *in* "The Chemistry of Transition Metal Carbides and Nitrides" (S. T. Oyama, Ed.), p. 1. Blackie Acad. & Prof., Glasgow, 1996.
10. Ledoux, M. J., Pham-Huu, C., and Chianelli, R. R., *Curr. Opin. Solid State Mater. Sci.* **1**, 96 (1995).
11. Pham-Huu, C., Ledoux, M. J., and Guille, J., *J. Catal.* **143**, 249 (1993).
12. Iglesia, E., Baumgartner, J. E., Ribeiro, F. H., and Boudart, M., *J. Catal.* **131**, 523 (1991).
13. Lee, J. S., Locatelli, S., Oyama, S. T., and Boudart, M., *J. Catal.* **125**, 157 (1990).
14. Ledoux, M. J., Pham-Huu, C., Dunlop, H., and Guille, J., *J. Catal.* **134**, 383 (1992).
15. Oyama, S. T., *Catal. Today* **15**, 179 (1992).
16. Keller, V., Wehrer, P., Garin, F., Ducros, R., and Maire, G., *J. Catal.* **153**, 9 (1995).
17. Iglesia, E., Ribeiro, F. H., Boudart, M., and Baumgartner, J. E., *Catal. Today* **15**, 307 (1992).
18. Ledoux, M. J., Pham-Huu, C., Dunlop, H., and Guille, J., *in* "Proceedings, 10th International Congress on Catalysis, Budapest, 1992" (L. Guczi, F. Solymosi, and P. Tétényi, Eds.), p. 955. Akad. Kiado, Budapest, (1992).
19. Blekkan, E. A., Pham-Huu, C., Ledoux, M. J., and Guille, J., *Ind. Eng. Chem. Res.* **33**, 1657 (1994).

20. Ledoux, M. J., Guille, J., Pham-Huu, C., Dunlop, H., and Prin, M., U.S. Patent 5,468,370.
21. Ledoux, M. J., Del Gallo, P., Pham-Huu, C., and York, A. P. E., *Catal. Today* **27**, 145 (1996).
22. Anderson, G., and Magneli, A., *Acta Chem. Scand.* **4**, 793 (1950).
23. Ledoux, M. J., Guille, J., Pham-Huu, C., Pechiera, E., and Blekkan, E. A., U.S. Patent 5,576,466.
24. Roy, S., Bouchy, C., Pham-Huu, C., Crouzet, C., and Ledoux, M. J., "Proceedings, AIChE 1998 Spring National Meeting" New Orleans, pp. B5–B10 (1998).
25. Ledoux, M. J., Pham-Huu, C., York, A. P. E., Blekkan, E. A., Delporte, P., and Del Gallo, P., *in* "The Chemistry of Transition Metal Carbides and Nitrides" (S. T. Oyama, Eds.), p. 373. Blackie Acad. & Prof., Glasgow, 1996.
26. Katrib, A., Logie, V., Peter, M., Wehrer, P., Hilaire, L., and Maire, G., *J. Chim. Phys.* **94**, 1923 (1997).
27. Burtch, R., and Mitchell, P. C. H., *J. Less-Common Metals* **54**, 363 (1977).
28. Matsuda, T., Shiro, H., Sakagami, H., and Takahashi, N., *Catal. Lett.* **47**, 99 (1997).
29. Boudart, M., and Leclercq, L., U.S. Patent 4,271,041.
30. Bouchy, C., Thèse de Chimie, Université L. Pasteur de Strasbourg (1998).
31. Glemser, O., and Lutz, G., *Z. Anorg. Allg. Chem.* **264**, 17 (1951).
32. Cirillo, A., and Fripiat, J., *J. Phys.* **3**, 247 (1978).
33. Gouin, X., Thèse de Chimie, Univ. de Rennes, pp. 114–115 (1993).
34. Marchand, R., Gouin, X., Tessier, F., and Laurent, Y., *in* "The Chemistry of Transition Metal Carbides and Nitrides" (S. T. Oyama, Eds.), p. 252. Blackie Acad. & Prof., Glasgow, 1996.
35. Hägg, G., *Z. Phys. Chem.* **12**, 33 (1931).
36. Ledoux, M. J., Pham-Huu, C., Meunier, F., Del Gallo, P., Krause, A. O. I., and Niemi, V., *in* "Book of Abstract 11th ICC, Baltimore 1996" (J. W. Hightower, W. N. Delgass, E. Iglesias, and A. T. Bell, Eds.), p. 361. Amer. Chem. Soc., Washington, DC, 1996.
37. Ledoux, M. J., Meunier, F., Heinrich, B., Pham-Huu, C., Harlin, M. E., and Krause, A. O. I., *Appl. Catal. A* **181**, 157 (1999).
38. Ferguson, I. F., Ainscough, J. B., Morse, D., and Millar, A. W., *Nature* **202**, 1327 (1964).
39. Lee, J. S., Volpe, L., Ribeiro, F. H., and Boudart, M., *J. Catal.* **112**, 44 (1988).
40. Meunier, F., Thèse de Chimie, Université L. Pasteur de Strasbourg (1995).
41. Yu, C. C., and Oyama, S. T., *J. Solid State Chem.* **116**, 205 (1995).
42. Oyama, S. T., Delporte, P., Pham-Huu, C., and Ledoux, M. J., *Chem. Lett., Chem. Soc. Jpn.* 949 (1997).
43. Martens, J. A., Jacobs, P. A., and Weitkamp, J., *Appl. Catal.* **20**, 239 (1986).
44. Boudart, M., and Ptak, L. D., *J. Catal.* **16**, 90 (1970).
45. Ribeiro, F. H., Ph.D. Thesis, Univ of Stanford, CA (1989).
46. (a) Engel, N., *Ingenioeren* N101 (1939); (b) Brewer, L., *Acta Metall.* **15**, 553 (1967).
47. Rappé, A. K., and Goddard, W. A., III, *J. Am. Chem. Soc.* **104**, 448 (1982).
48. Bursill, L. A., *Proc. R. Soc. A* **311**, 267 (1969).
49. Spevack, P. A., and McIntyre, N. S., *J. Phys. Chem.* **97**, 11031 (1993).
50. Martens, J. A., Souverijns, W., Verrelst, W., Parton, R., Froment, G. F., and Jacobs, P. A., *Angew. Chem., Int. Ed. Engl.* **34**, 2528 (1995).